Mechanical behaviour of SSRT specimens optimized for IGSCC concerns

Julien Deleume, Dominique Poquillon, Véronique Garat, Jean-Marc Cloué, Eric Andrieu

Mechanical behaviour of SSRT specimens optimized for IGSCC concerns

Julien Deleume [a,b,*], Dominique Poquillon [b], Véronique Garat [a], Jean-Marc Cloué [a], Eric Andrieu [b]

[a] AREVA, AREVA-NP, 10, rue J. Récamier, 69456 Lyon Cedex 06, France
[b] CIRIMAT, CNRS/UPS/INPT, ENSIACET, 118 Route de Narbonne, 31077 Toulouse Cedex 4, France

Abstract

Simulating testing conditions leading to evaluate the intergranular stress corrosion cracking sensitivity of structural alloys is crucial to estimate the lifetime of in-service components. Former studies have pointed out that a simple modification of the design of slow strain rate tensile specimens was particularly convenient for evaluating the susceptibility to intergranular stress corrosion cracking of nickel-base alloys. The aim of the present work is to characterize and model the mechanical behaviour of such specimens. Validation of proposed modelling relies mainly on tensile tests carried on specimens equipped with strain gages. One of the striking results is that, for a given displacement rate of the heads of the specimen, a much slower strain rate can be obtained locally in comparison with the strain rate of an equivalent smooth specimen.

Keywords: A. Nickel; A. Superalloys; B. Modelling studies; C. Effects of strain; C. Stress corrosion

1. Introduction

The family of nickel-base alloys, widely used in many industries (*e.g.* aeronautical, oil, marine, nuclear) since the very beginning of the 60s, is known to be sensitive to environmentally-induced intergranular stress corrosion cracking (IGSCC – see Fig. 1) [1–5]. Thus, as an example, alloy 600 has been studied intensively because of the widespread problems encountered with steam generators tubing [2,3,5]. In spite of numerous studies devoted to understanding and explaining mechanisms responsible for IGSCC, relatively little attention has been paid to define a specific test in order to evaluate the lifetime expectancy of in-service components. Indeed, conventional tests dedicated to SCC concerns, such as slow strain rate (SSR) and reverse U-bend (RUB) techniques, do not allow an understanding of the behaviour of components nor generate damage comparable to that induced by in-service conditions. Moreover, since they are defined with an imposed displacement and need very low experimental speeds (typically, strain rate of about $10^{-7}\ s^{-1}$), those tests are very time consuming and very difficult to perform. As a result, Totsuka et al. [6–8] have proposed an original design of slow strain rate tensile (SSRT) specimens which enables stressing of the sample surface.

SSRT tests were carried out on specimens with a "V"-shaped hump in the middle of the gauge length. They revealed to be a useful technique for evaluating susceptibility to IGSCC of alloy 600 tested in aqueous environments at intermediate temperature (300–400 °C) [6]. For this design and for tests carried out with an imposed strain rate of $5 \times 10^{-7}\ s^{-1}$, the fracture surface is always characteristic of IGSCC whereas it is not so on double notched SSRT specimens and never observed on conventional tensile specimens tested in the same experimental conditions. Results obtained from more recent studies have pointed out several

* Corresponding author. Address: AREVA, AREVA-NP, 10, rue J. Récamier, 69456 Lyon Cedex 06, France. Tel.: +33 (0) 472 747369; fax: +33 (0) 472 747325.
E-mail address: julien.deleume@wanadoo.fr (J. Deleume).

doi:10.1016/j.corsci.2007.10.007

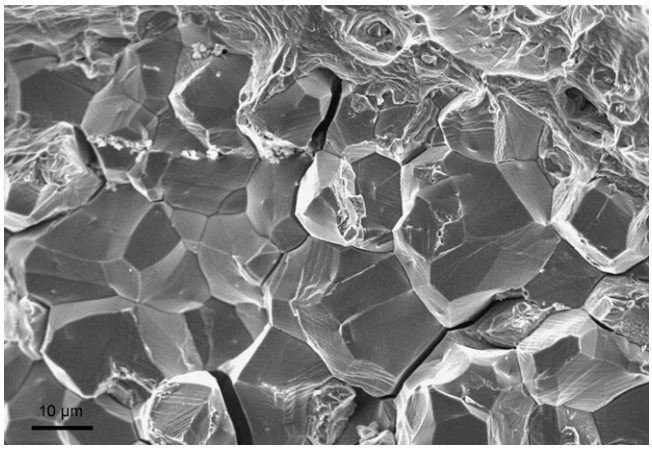

Fig. 1. SEM image of a typical fracture surface of a specimen tested under IGSCC conditions.

main facts concerning the behaviour of such a specimen design.

Boursier et al. [9] conclusively proved that such a particular geometry of SSRT specimens increases the crack initiation sensitivity together with the crack propagation. All the tested heats, including those known to be far less sensitive to IGSCC, exhibit an intergranular brittle fracture surface, due to the geometrical factors associated with the strain localization which remains constant during the test. Besides, in this particular geometry, the measured crack propagation rate in the apex of the "V" is higher than the one recorded on conventional tensile specimens and a hardness gradient was highlighted between the bulk material and the surfaces of the "V". Thanks to FEM calculations, the authors also showed that the specimen mechanical response is linked with alloy's work hardening: the higher the strain hardening is, the higher is the local strain rate in the apex of the "V". As a result, IGSCC would be due to the combined action of specimen geometrical factors and alloy's properties, provided a strain threshold of at least 40% is reached, whatever the origin of the initiation crack is.

In this study, the purpose is, on the one hand, to study the mechanical behaviour of these "V"-shaped specimens by using strain gages bonded on them. On the other hand, having a predictive finite element simulation of that kind of SSRT tests could facilitate and improve one's understanding of IGSCC mechanisms in nickel-base alloys.

2. Material and experimental procedures

As thin specimens were required, a 0.7 mm thick strip of alloy 718 (UNS NO7718) was used in this study. It was obtained through a double melting process: vacuum induction melting plus vacuum arc remelting. The nominal composition of the alloy is given in Table 1. Fig. 2 describes the dimensions of specimens used in this study. The "V" in the middle of their gauge length was made by cold stamping with a specific dye. Specimens were then heat treated under

Table 1
Chemical composition of alloy 718 (weight%)

Ni	Fe	Cr	Mo	Al	Ti	Nb	Ta	C
50–55	Bal.	17–20	3–3.5	0.2–0.8	0.7–1.2	4.7–5.5	0.1	<0.08

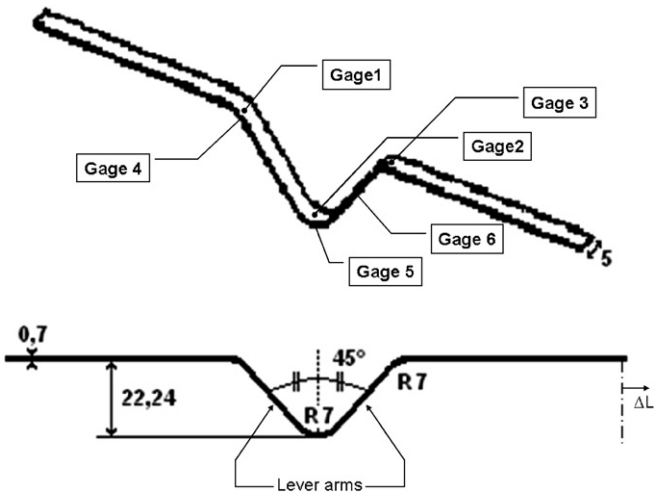

Fig. 2. Geometry of studied SSRT specimens. Specimen dimensions are given in mm.

Table 2
Grain size (ASTM grain size number) and mechanical properties (Young's modulus, yield strength, ultimate tensile strength, elongation to rupture and Poisson's ratio) as measured at room temperature

Grain size	YM (GPa)	YS (MPa)	UTS (MPa)	E (%)	PR
8–9	200	1396	1472	16.9	0.295

vacuum following the conventional aeronautical heat treatment: hold 720 °C – 8 h, cooling 50 °C/h down to 620 °C, hold 620 °C – 8 h followed by air quenching at room temperature. Grain size and room temperature mechanical properties of studied material are listed in Table 2.

Two types of tensile tests were carried out at room temperature under laboratory air on an Instron™ electromechanical machine with a 10 kN load cell:

- In the first case, the relative displacement of the lever arms was determined through the use of a laser micrometer by measuring the distance between two alloy 718 flags spot welded on the lever arms of the "V" (Fig. 3). The mechanical test was performed with an imposed displacement rate (dL/dt) of 1 mm per minute.
- In the other case, instantaneous local strains in the shoulders and at the tip of the "V" were measured by Vishay™ EA-06-062AP-120 uniaxied strain gages with a strain range of ±3% for a gauge length of 0.62 mm. The layout of the strain gages is given on Fig. 2 (gages labelled from 1 to 6). Two tests were performed at different imposed displacement rate, respectively, 1 and 2 mm per minute.

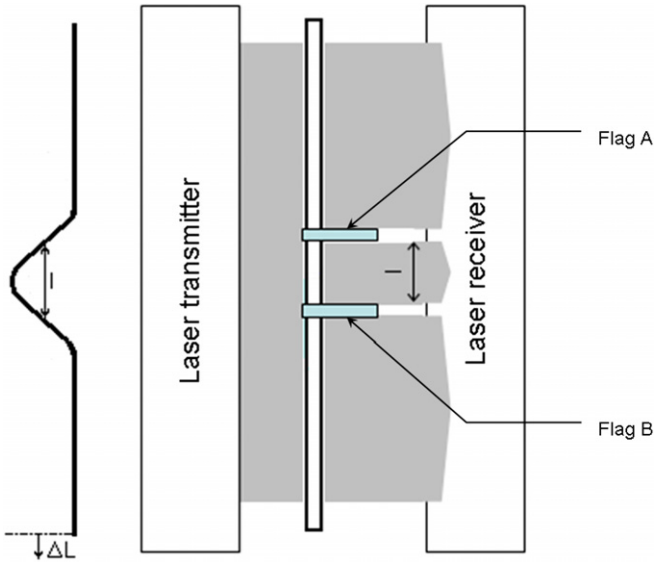

Fig. 3. Front and side views of the tested specimen showing the laser beam, the flags location and gauge length dimension ($L_0 = 30$ mm).

Finite element calculations have been carried out to determine the local stress and strain tensor fields scale and distribution in the specimen. Cast3m finite element code [10] was used. A 2D modelling (8 node quadratic elements) with plane strain hypothesis was chosen because of the width of the SSRT sample. Furthermore, the symmetry of the problem allows us to mesh only half of the specimen. An isotropic elastoplastic mechanical behaviour was chosen to describe the flow rule. In the code, this mechanical behaviour with non linear hardening enables to fit the true stress–strain curve (Fig. 4).

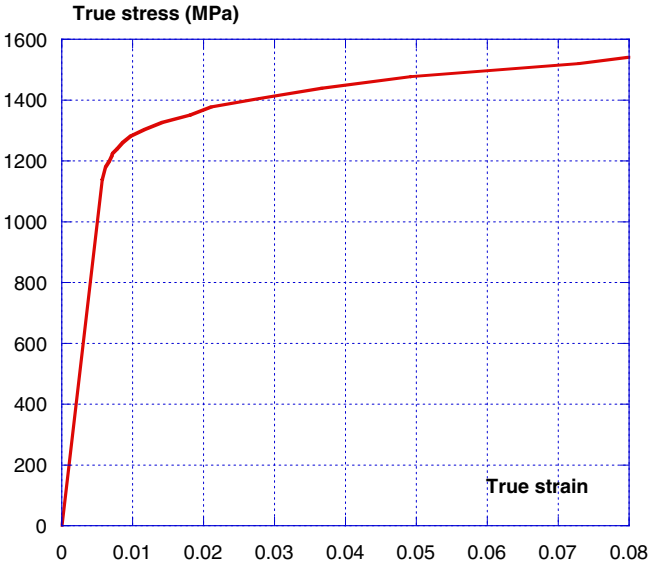

Fig. 4. Representative room temperature experimental tensile curve (true stress, true strain) corresponding to the material of this study (20 °C, $\frac{d\varepsilon}{dt} = 10^{-3}$ s^{-1}). FEM simulations rely on this curve (plasticity begins for a stress equal to 1139 MPa then non linear hardening).

3. Results

Experimental data and simulations are compared from a macroscopic point of view using the data given by the laser extensometer that measures the distance between flags A and B spot welded on the lever arms of the specimen as shown on Fig. 3. On the one hand, the specimen elongation is a linear function of the displacement. On the other hand, numerical simulation is in good agreement with experimental data (Fig. 5). The specimen opens out during the test (Fig. 6) and the opening of the lever arms is linked to the geometrical specificity of the sample (angle and length of the lever arms, curvature radius and angle of the "V"-shaped part of the specimen). If the lever arms are supposed to open out rather than to stretch, then, a geometrical analytical relation can be derived between the global imposed displacement (ΔL) and the opening of the "V" (Δl). In the case of the present test, the initial distance between the extremities of the "V"-shaped part of the specimen is 44.48 mm and the extensometer basis (l) is 30 mm.

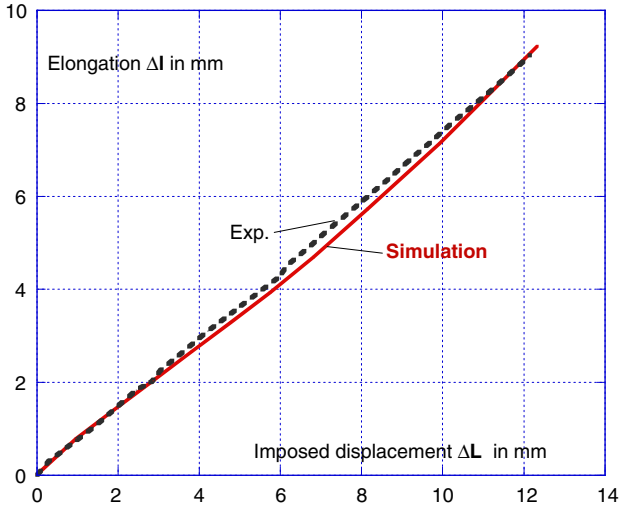

Fig. 5. Elongation Δl measured in the "V"-shaped part of the specimen (see Fig. 3). Comparison between experimental data and FEM calculations.

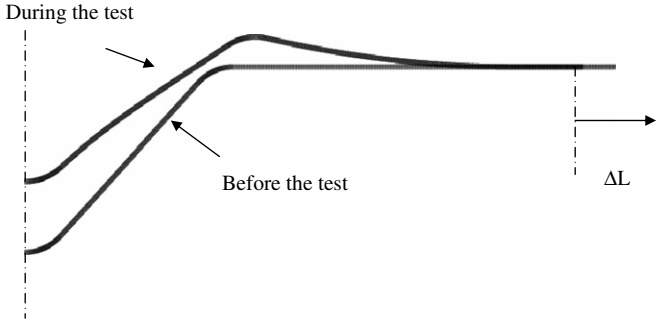

Fig. 6. Calculated shape of the SSRT specimen before and after an imposed displacement $\Delta L = 4.8$ mm. Note that the lever arms behave elastically.

The predicted ratio between elongation (Δl) and imposed displacement (ΔL) is $\beta = 44.48/30 = 1.48$. The slope of the curves on Fig. 5 is 1.3 which is in good agreement with the simplified approach. This difference comes from the elastic stretching of the lever arms taken into account in the finite element calculations, which are in perfect agreement with the experimental data.

As this type of specimen is designed for IGSCC concerns, it is now useful to consider the local aspect of the mechanical fields and more especially to compare the measured and the calculated strain maps. The first point to be noted is that no significant difference appears between tests carried out at the two different imposed displacement rates: $\frac{dL}{dt} = 1$ mm per minute and $\frac{dL}{dt} = 2$ mm per minute. As the specimen is blocked on one side and the displacement imposed on the other, comparing gages 1 and 3 enables to check the symmetry of the problem. In both tests, the data collected indicate the same strain. The third point consists in the comparison of the gages located on the extrados and the intrados of the apex of the "V"-shaped part. For gages 2 and 5, the amplitude of the strain in the intrados is always slightly higher than in the extrados as expected and calculated (because of a smaller curvature radius). The same remark can be done for gages 1 and 4 in the shoulder (Fig. 7). The intrados areas are subjected to tension whereas the extrados areas are subjected to compression.

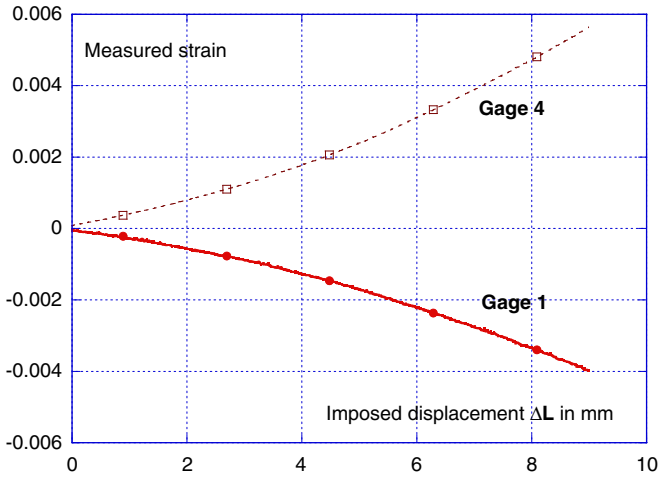

Fig. 7. Measured strain as a function of the imposed displacement ΔL. See Fig. 2 for gages location.

The unique feature of this type of specimen is to localize the tensile stress where gage 2 is located (*e.g.* in the intrados of the "V"). Fig. 8 gives a zoom on this part of the sample and finite element calculations show two interesting points. In the apex of the "V", the strain gradient is important in the thickness of the specimen, but in the same time, the strain changes very slowly in the length of the specimen. The consequences of theses points will be detailed in the discussion.

Fig. 9 compares the evolution of measured and calculated strain for gages 2 and 5. The agreement is good, computations tend to underestimate the traction in the intrados

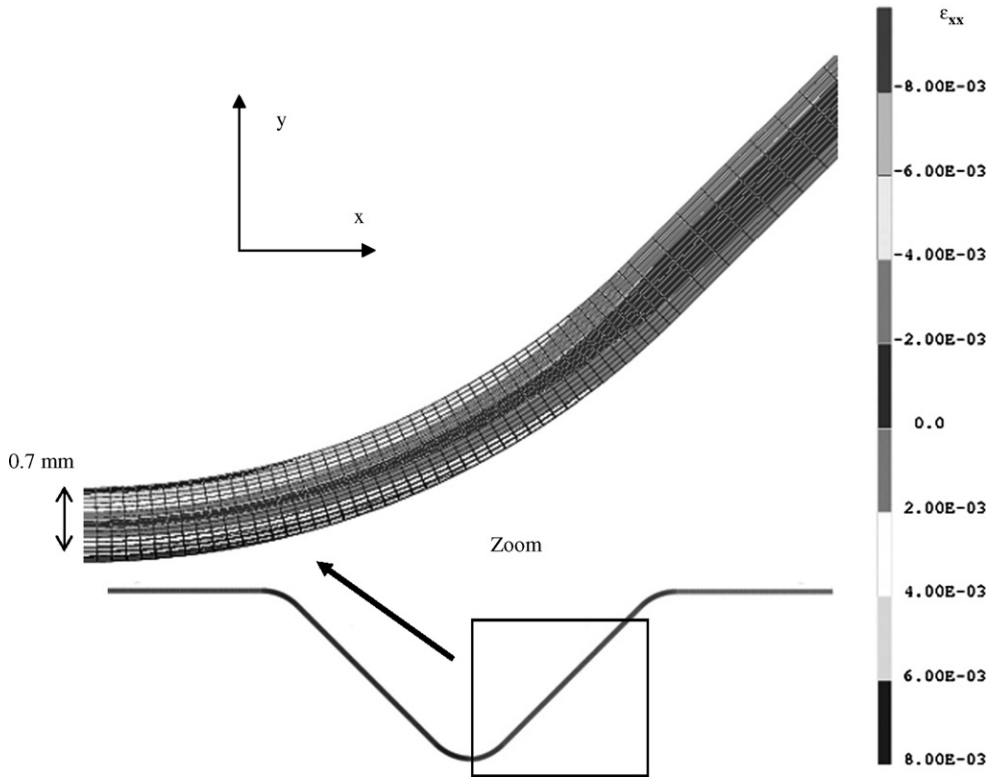

Fig. 8. Calculated strain ε_{xx} for a 6.8 mm imposed displacement.

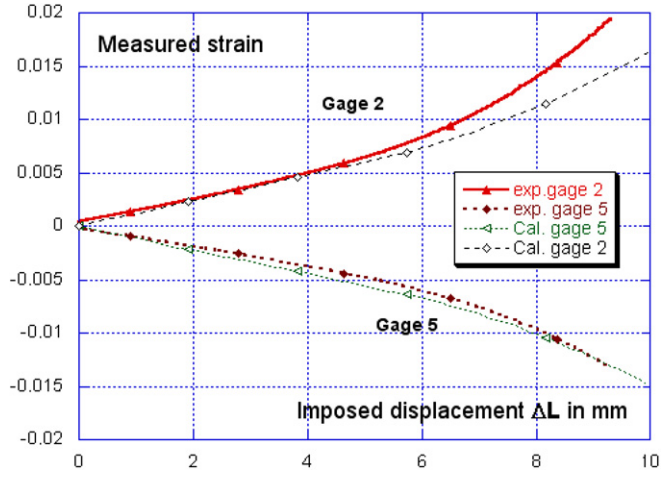

Fig. 9. Measured strain as a function of the imposed displacement ΔL. Comparison between experimental data and FEM calculations. See Fig. 2 for gages location.

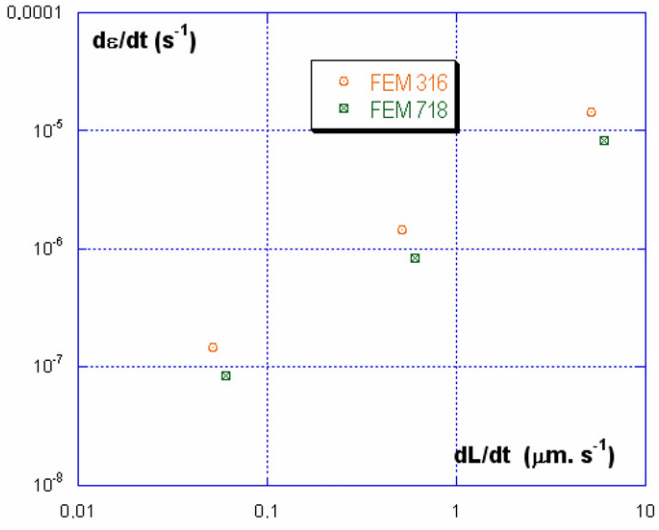

Fig. 10. Maximal strain rate $\frac{d\varepsilon}{dt}$ in the intrados of the tip of the "V" for an imposed displacement rate $\frac{dL}{dt}$. FEM calculations are compared with the average strain rate reached for $\Delta L = 6$ mm for the material of this study (FEM 718) and for 316 LN stainless steel with stress hardening at 600 °C (FEM 316).

compared to the experimental results, but the isotropic elastoplastic model used does not take into account the residual stresses which may remain in the specimen at the beginning of the test and the influence of the previous compression on the behaviour of the material in traction. However, as the shaping step of the specimen is followed by a high temperature heat treatment to reinforce the alloy by precipitation of γ' and γ'' phases, one can expect a relaxation of most of internal stresses.

During the first 8 mm of the imposed displacement L, which correspond to the opening of the lever arms, strain is about 10 times higher in the intrados of the "V" than in the arms which behave elastically. The strain measured on gage 6 confirms the results of the calculations. The analysis of the macroscopic elongation is then confirmed and the dominant effect is the opening of the lever arms rather than their stretching. A good control of the imposed strain rate in the tip of the "V"-shaped part of the specimen is then possible.

4. Discussion

For SCC concerns, $10^{-7}\ \mathrm{s}^{-1} \leqslant \frac{d\varepsilon}{dt} \leqslant 10^{-5}\ \mathrm{s}^{-1}$ is a typical range of strain rates which imposes the use of specific SSRT testing machines. In the case of the "V"-shaped geometry used in the present study, an imposed displacement rate $\frac{dL}{dt} = 0.1\ \mu\mathrm{m\ s}^{-1}$ is enough to reach locally the lowest strain rate value (*e.g.* $10^{-7}\ \mathrm{s}^{-1}$), thanks to the specific geometry of the specimens. In comparison, the same imposed displacement rate $\frac{dL}{dt}$ for a conventional tensile specimen leads to nearly thirty times higher imposed strain rate of about $\frac{d\varepsilon}{dt} = 3 \times 10^{-6}\ \mathrm{s}^{-1}$. Fig. 10 shows strain rates calculated by FEM simulation in the intrados of the tip of the "V". On this graph, results of FEM calculations for a 316 LN stainless steel at 600 °C were added. In this material, strain hardening is larger than in alloy 718 at room temperature and its elastoplastic behaviour can be modelled using a Ramberg–Osgood law as in [11]

$$\varepsilon = \varepsilon_{\mathrm{el}} + \varepsilon_{\mathrm{pla}} = \frac{\sigma}{E} + \alpha \cdot \sigma^{n} \qquad (1)$$

with stresses given in MPa, Young's modulus $E = 144$ GPa, $n = 2.5$ and $\alpha = 6.9 \times 10^{-8}$. For materials with larger strain hardening like 316 LN stainless steel at 600 °C, the FEM calculated strains are slightly larger than the prediction of the analytical approach due to less localized strain.

One should also focus on the local strain field in the tip of the "V" with respect of specimen thickness. Indeed, if considering Fig. 9, the intrados of the tip of the "V" is subjected to tension whereas the extrados is subjected to compression. This variation of the strain in specimen thickness is not far from a linear function, whereas it remains very homogeneous in planes parallel to the neutral fibre. For instance, for an imposed displacement of 4 mm, gage 2 gives a strain of about $\varepsilon = 5 \times 10^{-3}$ and gage 5 a strain of about $\varepsilon = -5 \times 10^{-3}$. This variation of strain takes place in a thickness of about 0.7 mm, hence a 10% loss of strain reached in less than 35 μm in the intrados of the tip of the "V". This value is comparable to the double of the average grain size of studied material.

All those facts conclusively prove that, as suggested by Totsuka et al. [6], this specific SSRT specimen geometry is both perfect to localize strain and to control it with a high accuracy. Moreover, thanks to that particular design, the zone where the strain rate is both homogeneous and maximum in the intrados of the tip of the "V" covers several square millimetres.

It is also of relevant interest to study the effect of strain hardening on the mechanical behaviour of such SSRT

specimens, as studied by Boursier et al. [9]. As the specimen forming is made by cold stamping with a specific dye, a local hardening of the material occurs, especially in the "V"-shaped part of the specimen. That local hardening can be approximated by the ratio e/R which is equal to $0.7/7 = 10\%$ for the studied geometry. Since the forming of the specimen is made before the ageing heat treatment, the local hardening of alloy in cold stamped areas at the beginning of the tests could not be higher than 10%. This statement has been confirmed by complementary electron backscatter diffraction characterizations of the local plastic strain carried out on specimens after age hardening heat treatment, according to the Lehockey et al.'s method [12,13]. Strains are not significantly different on each side of the "V" after the age hardening treatment. Moreover, tensile tests have been carried out at room temperature on specimens submitted to an imposed plastic pre-deformation comparable to the one induced by cold stamping. Mechanical properties of pre-deformed material differ slightly from those of non pre-deformed material. Thus, a maximal shift of about 40 MPa is observed on the yield strength value whereas the plastic part of the tensile curves remains similar in both cases, hence no significant effect of local strain hardening on the global mechanical behaviour of the specimen.

Finally, it is not yet clear whether the capacity of such SSRT tests to generate intergranular brittle fracture is simply due to the very slow imposed strain rate or if it results of the combined action of strain rate and lever arms effect. Complementary tests are in progress and preliminary results prove that the observed fracture mode depends of the imposed strain rate. Indeed, for strain rates higher than $10^{-6}\,s^{-1}$, the fracture surface of "V"-shaped specimen remains totally transgranular ductile, whereas, for lower strain rates, intergranular brittle areas are observed. It is then likely that the key point to be compatible with IGSCC occurrence is a slow enough strain rate. Moreover, another question is raised by such an assumption. Indeed, one could not exclude that the intergranular brittle character of observed fracture surface may be linked with a change in deformation mechanisms. Considering the works of Kergaravat et al. [14] and Noel et al. [15], nickel-base alloys; namely, alloy 600 and alloy 690, can exhibit grain boundary sliding (GBS) at intermediate temperature (300–500 °C). Even if correlations between GBS and IGSCC resistance have been highlighted, the involved mechanisms are still subject to controversy. Numerous other factors can play a predominant role (such as grain boundary structure, Taylor/Schmitt factor generated by texture). Consequently, further investigations have to be carried out so as to improve one's understanding of those phenomena.

5. Conclusion

Based on both complementary tensile tests and finite element calculations, this study conclusively proves that the original design of SSRT specimens due to Smialowska et al.'s work [6–8] is of relevant sensitivity for IGSCC concerns. Indeed, that geometry is both useful to localize strain and to control it with a high accuracy. Furthermore, the range of strain rates that develop along gradients in such geometry cannot be achieved with smooth specimens. The most striking conclusion which can be drawn from the present work is that a wide range of local strain rate can be tested for an imposed displacement rate, owing to adaptations of the specific geometrical parameters of SSRT specimen. In fact, the key feature is that the design relies on the lever arms length which enables, even on a conventional tensile testing machine, to carry out SSRT tests with strain rates far lower than those imposed with specific equipment. This study has huge practical implications: it would allow thresholds (in strain rate dependence) that give rise to changes in corrosion effects (transgranular to intergranular morphology) to be identified without a large matrix of specimen/testing. This can be extremely important when understanding factors that impact susceptibility to SCC nucleation (versus propagation). However, the specific sample geometry can limit this kind of test to flat products which can be shaped, stress-relieved without significant microstructure modifications.

Acknowledgements

The authors are grateful to D. Falandry for tensile tests performed on specimens equipped with strain gages (CRITT Mécanique et Composites de Toulouse, France) and to B. Brugier and C. Grosjean for the EBSD analysis. They also would like to acknowledge AREVA-NP company for its financial support.

References

[1] M.T. Miglin, H.A. Domian, J. Mater. Eng. 9 (1987) 113–132.
[2] R.H. Jones, S.M. Bruemmer, in: EICM Proceedings, 1988, pp. 287–310.
[3] G.S. Was, Corrosion 46 (4) (1990) 319–330.
[4] M.O. Speidel, R. Magdowski, in: Proceedings of the Sixth International Symposium on Environmental Degradation of Materials in Nuclear Power Systems – Water Reactors, 1993, pp. 361–376.
[5] P.M. Scott, Int. J. Press. Ves. Pip. 65 (1996) 255–264.
[6] N. Totsuka, E. Lunarska, G. Cragnolino, Z. Szklarska-Smailowska, Scripta Metall. 20 (1986) 1035–1040.
[7] N. Totsuka, E. Lunarska, G. Cragnolino, Z. Szklarska-Smailowska, Corrosion 43 (8) (1987) 505–514.
[8] N. Totsuka, Z. Szklarska-Smialowska, Corrosion 43 (12) (1987) 734–738.
[9] J.M. Boursier, J.P. Saulay, Y. Bréchet, G. Zacharie, in: Colloque Matériaux 2002, Session 5 : Corrosion et anti-corrosion dans les installations industrielles, Tours, France, October 21–25, 2002.
[10] Cast3M, <http://www-cast3m.cea.fr/cast3m/index.jsp>.
[11] R. Piques, Mécanique et mécanismes de l'amorçage et de la propagation des fissures en viscoplasticité dans un acier inoxydable austénitique, Ph.D. thesis, Ecole Nationale Supérieure des Mines de Paris, France, 1989.

[12] E.M. Lehockey, A.M. Brennenstuhl, I. Thompson, Corros. Sci. 46 (2004) 2383–2404.
[13] E.M. Lehockey, Y.P. Lin, O.E. Lepik, Mapping residual plastic strain in materials using EBSD, in: A.J. Schwartz, M. Kumar, B.L. Adams (Eds.), Electron Backscatter Diffraction in Materials Science, Kluwer Academic Pub., New York, 2001, pp. 247–264.
[14] J.-F. Kergaravat, X. Ballin, G. Robert, in: Second International Conference on Corrosion–Deformation Interactions, 1996.
[15] D. Noel, O. de Bouvier, F. Foct, T. Magnin, J.D. Mithieux, F. Vaillant, in: Proceedings of the Second International Conference on Corrosion–Deformation Interactions, 1996, pp. 435–452.